Charge-Order-Induced Ferroelectricity in LaVO_{3}/SrVO_{3} Superlattices

Se Young Park, Anil Kumar, and Karin M. Rabe

Phys. Rev. Lett. **118**, 087602 — Published 24 February 2017

DOI: 10.1103/PhysRevLett.118.087602

Charge-order-induced ferroelectricity in $LaVO_3/SrVO_3$ superlattices

Se Young Park,[1,*] Anil Kumar,[2] and Karin M. Rabe[1]

[1]*Department of Physics & Astronomy, Rutgers University, Piscataway, NJ 08854, USA*
[2]*Theoretical Division, Los Alamos National Laboratory, NM 87545, USA*

The structure and properties of the 1:1 superlattice of $LaVO_3$ and $SrVO_3$ are investigated with a first-principles density-functional-theory-plus-U (DFT+U) method. The lowest energy states are antiferromagnetic charge-ordered Mott-insulating phases. In one of these insulating phases, layered charge ordering combines with the layered La/Sr cation ordering to produce a polar structure with a large nonzero spontaneous polarization normal to the interfaces. This polarization, comparable to that of conventional ferroelectrics, is produced by electron transfer between the V^{3+} and V^{4+} layers. The energy of this normal-polarization state relative to the ground state is only 3 meV per vanadium. Under tensile strain, this energy difference can be further reduced, suggesting that the normal-polarization state can be induced by an electric field applied normal to the superlattice layers, yielding an antiferroelectric double-hysteresis loop. If the system does not switch back to the ground state on removal of the field, a ferroelectric-type hysteresis loop could be observed.

PACS numbers: 73.21.Cd, 75.25.Dk, 77.55.Px

The identification of novel mechanisms for ferroelectricity and discovery of their materials realizations has attracted much interest in recent years. One general approach, proposed by Khomskii[1, 2] is to combine two symmetry-breaking orderings, neither of which separately lift inversion symmetry, to generate a switchable polar structure [3]. In perovskite oxides, development of the layer-by-layer growth techniques [4–6] offers controlled symmetry breaking by cation layering [7–13]. (Multi)ferroelectricity in oxide superlattices can then achieved by a second symmetry-breaking lattice distortion, either an oxygen-octahedron rotation pattern or Jahn-Teller-type oxygen-octahedron shape distortion [3, 14–17]. Symmetry breaking by charge disproportionation and ordering [18] has, in contrast, been much less explored [2, 19–22]. Charge-ordering-ferroelectricity can in principle achieve a large switching polarization due to the motion of charge across the unit cell in the transformation between two variants [23], and could reduce the time scale of switching to characteristic electronic rather than lattice time scales [24].

In perovskite transition metal (TM) oxide $(ABO_3)_n(A'BO_3)_m$ (001) superlattices, the layered A/A′ cation ordering lowers the symmetry from cubic to tetragonal and breaks up-down symmetry across BO_2 layers. Control of the TM d-orbital occupancy through choice of A cations and layer thicknesses to obtain a mixed valence leads to charge disproportionation and long-range charge ordering [13, 16, 18, 25]. As we will discuss further below, layered charge ordering breaks the up-down symmetry across the AO and A′O layers. Thus, the combination of these two symmetry-breaking orderings (TM site-centered charge ordering and layered A-site cation ordering) can generate a switchable polar structure with polarization normal to the layers.

A 1:1 superlattice composed of $LaVO_3$ and $SrVO_3$ is a promising candidate for this type of charge-order-induced ferroelectricity. The low temperature phases of orthorhombic $LaVO_3$ and cubic $SrVO_3$ are antiferromagnetic Mott-insulating and correlated metallic, respectively [18, 26–28]. When they form the 1:1 superlattice, the average valence of the vanadium has a fractional value of +3.5. Due to the strong on-site Coulomb interaction, the Mott-insulating state with charge, orbital, and magnetic order would be preferred where the vanadiums disproportionate so that half of the vanadium cations have nominal valence V^{3+} and the other half V^{4+} [29, 30].

In this paper, we use first-principles total energy calculations to investigate the low-energy charge-ordered phases of the $(LaVO_3)_1(SrVO_3)_1$ superlattice. We show that there are three competing low-energy phases with distinct charge-order patterns, one of which is a layered charge ordering, and analyze the density of states and local structure. The epitaxial strain dependence of the relative energies is computed. For the polar structure generated by the layered charge order, we compute and discuss the spontaneous polarization normal to the layers, and predict the stabilization of this phase by an applied electric field.

We performed first-principles density-functional-theory calculations with the generalized gradient approximation plus U (GGA+U) method using the Vienna *ab-initio* simulation package [31, 32]. The Perdew-Becke-Erzenhof parametrization [33] for the exchange-correlation functional and the rotationally invariant form of the on-site Coulomb interaction [34] are used with $U = 4$ eV and $J = 0.6$ eV for the vanadium d states [51][35–37] and $U_f = 11$ eV and $J_f = 0.68$ eV for the La f states to shift the La f bands away from the Fermi energy [38]. We used the projector augmented wave method [39] with an energy cutoff of 600 eV and k-point sampling on a $4\times4\times4$ grid with a $2\times2\times2$ unit cell chosen to accommodate the relevant octahedral rotation distortions and charge-order patterns. The ferroelectric polarization was calculated using the Berry phase method [40] with $6 \times 6 \times 4$ k-point grid.

To determine the lowest-energy crystal structures and magnetic orderings of the 1:1 superlattice shown in Fig. 2(a), we first observe that with average valence +3.5, the vanadium ions are expected to disproportionate to V^{3+} and V^{4+}. We considered the three cell-doubling charge-order patterns il-

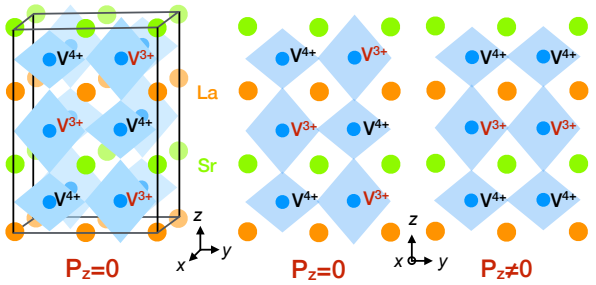

FIG. 1: (Color online) Schematics of the charge-order patterns for $(LaVO_3)_1/(SrVO_3)_1$ superlattice. For descriptive purposes the octahedral rotations and tilts are omitted and the Jahn-Teller distortions are exaggerated. The left, middle, right panels denote the checkerboard-type charge order with the (π, π, π) ordering vector, the stripe charge order with the $(0, \pi, \pi)$ ordering vector, and the layered charge order with the $(0, 0, \pi)$ ordering vector, respectively.

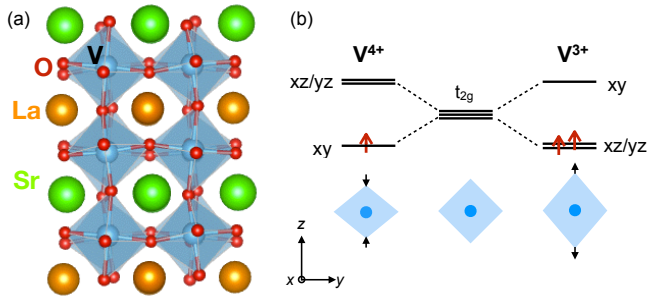

FIG. 2: (Color online) (a) Atomic arrangement in the $(LaVO_3)_1/(SrVO_3)_1$ superlattice. (b) The Jahn-Teller distortions and t_{2g} level splittings for V^{4+} (left) and V^{3+} (right).

lustrated in Fig. 1. In checkerboard charge ordering (CCO), which is the most common ordering in transition metal perovskite oxides [41], all the nearest-neighbor B sites of V^{4+} are V^{3+} and vice versa. In stripe charge ordering (SCO), the nearest-neighbor B sites of V^{4+} (V^{3+}) are V^{4+} (V^{3+}) in the x direction and V^{3+} (V^{4+}) in the y and z directions, forming a 2D y-z checkerboard with vanadium ions of a given valence forming lines along the x-direction. In layered charge ordering (LCO), planes of V^{4+} and V^{3+} alternate along the z-direction. We used the stacking method [42] to identify the oxygen octahedron rotation patterns of starting structures. Specifically, since bulk $SrVO_3$ has the cubic perovskite structure and bulk $LaVO_3$ has an orthorhombic $Pbnm$ structure with a $a^-a^-c^+$ rotation pattern [26, 27], we imposed the latter rotation pattern in two inequivalent orientations: one with the c axis along the z-direction (c oriented) and the other with the c axis along the x-direction (ab oriented).

For each starting structure, we fully relaxed the lattice constants and atomic positions for each of four magnetic orderings (ferromagnetic (F) and antiferromagnetic G-AFM, A-AFM and C-AFM). All relaxed structures are found to be insulating with a band gap larger than 1 eV. In all cases, the relaxed lattice has orthorhombic symmetry with lattice vectors close to cubic; for example, the lattice constants for c oriented LCO with C-AFM ordering are $a = 5.65$ Å, $b = 5.62$ Å, and $c = 7.83$ Å for the 20 atom cell; full structural and energetic information is given in the Supplementary Material. The energy difference between the two oxygen octahedron rotation patterns for a given charge and magnetic ordering is found to be small compared to the charge and magnetic ordering dependence; in what follows, we discuss c-oriented patterns.

Analysis of the relaxed structures shows that each valence state is found to drive a corresponding Jahn-Teller distortion of its coordinating oxygen octahedron. Specifically, in Fig. 3 we compare the V-O bond lengths of the V^{3+} and V^{4+} octahedra of the three charge ordering patterns with C-AFM magnetic ordering. The geometry of the in-plane oxygen positions is close to square and is the same for all vanadium atoms, independent of valence and charge ordering. The elongation in the apical direction for V^{3+} and contraction and off-centering for V^{4+} depend only on the valence and are nearly independent of the charge ordering, suggesting that these distortions are driven by orbital ordering of the vandadiums [16–18, 25, 43–45], as shown in Fig. 2(b). Elongation/contraction along the z axis is found to be energetically favorable for the charge orderings considered (see Supplementary Material Section VI).

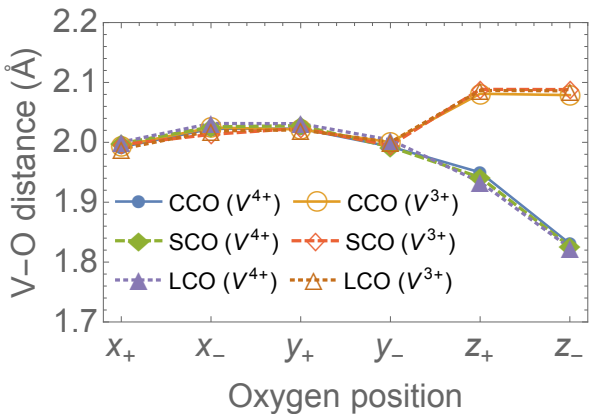

FIG. 3: (Color online) Distance between V and neighboring O atoms of V^{4+} and V^{3+} cations compared for CCO, SCO, and LCO phases. the labels $x_\pm$, $y_\pm$, and $z_\pm$ designate oxygen atoms by their octahedron positions in the high-symmetry ideal-perovskite reference structure to which the actual structure is related by small distortions.

Fig. 4 shows the total energies for the various magnetic orderings of each charge ordering pattern. The C-AFM ordering has the lowest energy for all three patterns, though for the CCO phase, the total energies of A-AFM and FM ordering are very close to that of C-AFM. It is remarkable that the energy differences between the lowest energy CCO, LCO, and SCO phases are quite small, with SCO computed to be lower in energy than LCO by only 3 meV per vanadium (in the Supplementary Material it is shown that this result is robust against the precise choice of the parameter U). This is much smaller than the classical electrostatic energy differences between cor-

responding arrangements of 3+ and 4+ point charges in a fixed compensating background, suggesting that there is substantial screening by the other charges in the system.

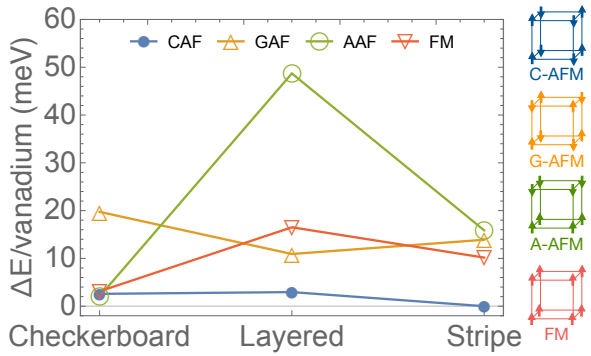

FIG. 4: (Color online) Total energy with respect to the lowest-energy configuration versus the charge ordering and magnetic ordering patterns. The symbols G, C, A, and FM represent the type of magnetic ordering of V-cations illustrated in the right column.

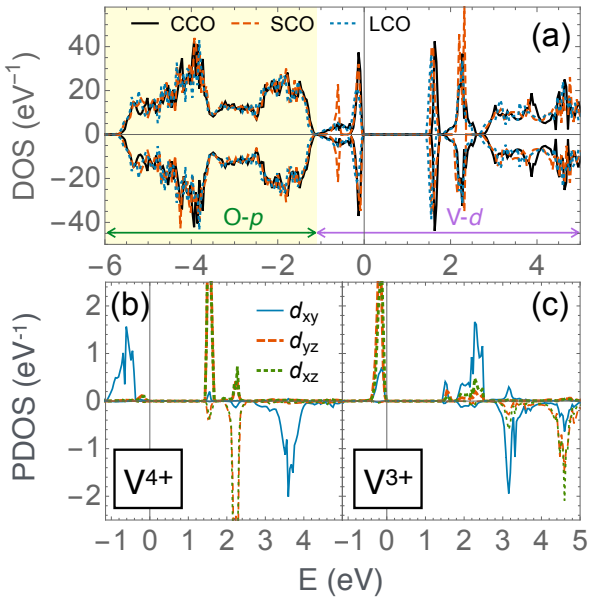

FIG. 5: (Color online) (a) Density of states of CCO (black solid line), SCO (red dashed line), and LCO (blue dotted line) phases with C-AFM ordering. The positive and negative sign of the vertical axis correspond to spin up and down states. The shaded (from -6 eV to -1.15 eV) and unshaded regions (from -1.15 eV to 5 eV) are oxygen p- and vanadium d-derived states, respectively. (b-c) PDOS in the LCO phase with C-AFM ordering for V t_{2g} with positive magnetic moment. (b) PDOS of the contracted octahedron (V^{4+}) with spin up polarization. (c) As in (b), on the elongated octahedron (V^{3+}).

The densities of states (DOS) of the superlattice in CCO, SCO, and LCO phases with C-AFM ordering are shown in Fig. 5 (a). Consistent with the small energy difference between the phases, they are almost identical, the main difference being in the occupied d_{xy} states, with a sharp peak for SCO and a broader distribution for CCO and LCO. The effect of the Jahn-Teller distortion can be seen from the projected density of states (PDOS), shown here for the LCO pattern (again, the corresponding PDOS for the other two phases are almost identical except for the occupied d_{xy} states as noted above). For the contracted octahedron (panel (b)) the occupied V-derived t_{2g} states have xy orbital character with full spin-polarization with xz/yz states lying about 1.5 eV above the Fermi energy. For the elongated octahedron (panel (c)), the xz and yz orbitals are occupied with empty xy states. The site-projected magnetic moment for the contracted and elongated octahedra are $1.02\mu_B$ and $1.78\mu_B$, respectively. Since the occupied d-states are fully spin polarized, the site-projected magnetic moments are close to the d-occupancy. This, in addition to the Wannier function analysis [46] showing an extra occupied Wannier function on the V ion with the larger magnetic moment (see Supplementary Material Section V), supports the identification of V^{4+}/V^{3+} valence states.

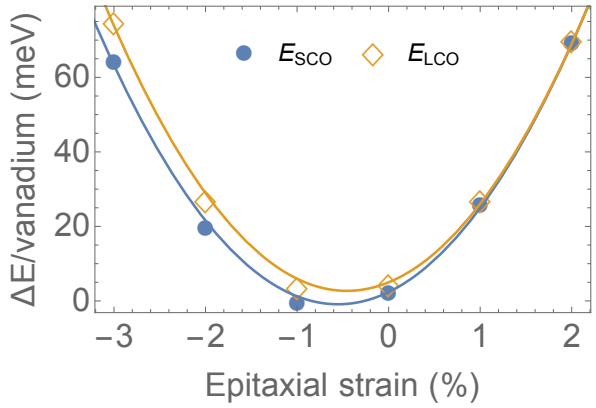

FIG. 6: (Color online) Total energy per vanadium with respect to the lowest energy configuration as a function of (001) epitaxial strain. The lines are obtained from quadratic fits to the data points. The zero-strain in-plane lattice constant is taken as the cube root of the volume of bulk $LaVO_3$ per f.u. obtained from the GGA+U calculation.

Next, we consider the symmetry and electric polarization of the various phases. The layered A-site cation ordering in the 1:1 superlattice lowers the cubic symmetry of the ideal perovskite structure to tetragonal $P4/mmm$ (#123). A c-oriented oxygen octahedron rotation pattern, combined with the layered A-site cation ordering, produces a $Pb2_1m$ (#26) structure with a small in-plane electric polarization resulting from non-cancellation of alternating A and A′ in-plane displacements [15, 16]; the computed value for the systems considered here is close to 4 μC/cm^2 (see Supplementary Material). A CCO charge ordering pattern lowers the symmetry further. The resulting $P2_1$ (#4) space group contains a reflection in z $(\bar{x}, y + \frac{1}{2}, \bar{z})$ and thus the out-of-plane polarization is zero by symmetry. The SCO charge ordering in the $Pb2_1m$ (#26) structure results in the space group Pn (#7) which con-

tains a reflection in z $(x+1/2, y+1/2, \bar{z})$ and thus has zero out-of-plane polarization. In contrast, LCO charge ordering results in the space group Pb (#7) with $(\bar{x}, y+\frac{1}{2}, z)$, which allows a nonzero polarization along z. We obtain the spontaneous polarization of the LCO phase by comparing the polarization change between two symmetry variants related by the operation $(\bar{x}, y+1/2, \bar{z})$, interpreted using a Wannier center analysis (Supplementary Material Section V). The change arises primarily from uniform transfer of electrons from V^{3+} to V^{4+}, which give a value of 29 μC/cm^2 if the transfer is across the LaO plane and 22 μC/cm^2 if the transfer is across the SrO plane. Adding the contributions from small displacements of the oxygen ions and associated Wannier centers, we obtain 34 and 17 μC/cm^2, the corresponding values obtained by Berry phase computed with appropriate branch choices. While for most ferroelectric systems, the choice of branch predicting the measured spontaneous polarization is clear [47], this system is unusual in that both choices are valid; this and other subtleties of the polarization in this system will be further discussed elsewhere [48].

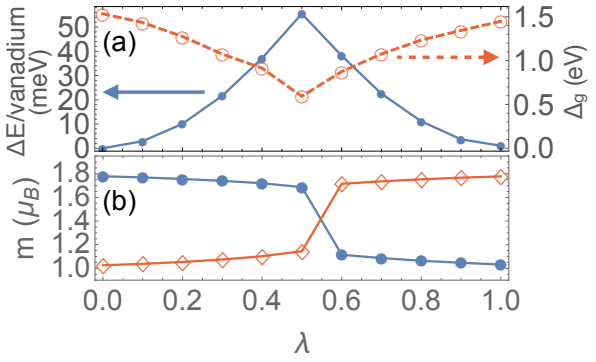

FIG. 7: (Color online) (a) Total energy per vanadium (blue solid line) with respect to the lowest energy configuration and band gap (red dashed line) for structures linearly interpolated between the SCO phase ($\lambda = 0$) and the LCO phase ($\lambda = 1$). (b) λ dependence of magnetic moments of the two V ions that have different nominal valence in SCO and LCO.

The epitaxial strain dependence of the energies of the SCO and LCO phases with C-AFM magnetic ordering is shown in Fig. 6. We find that the energy difference increases with compressive strain, while for tensile strain above 1%, it is close to zero. This suggests that in films under tensile strain, the polar LCO phase could be induced by an applied electric field normal to the layers, and a antiferroelectric double hysteresis loop could be observed for polarization normal to the layers. It is also possible that if the LCO phase does not switch back to the ground-state SCO phase on removal of the field, the system would exhibit a pseudo-ferroelectric hysteresis loop.

To investigate the energetics of the coupling between charge ordering and crystal structure, we computed the energy, band gap, and magnetic moments for structures obtained from a linear interpolation between the SCO ($\lambda = 0$) and the LCO ($\lambda = 1$) phase at 1% tensile strain, with results shown in Fig. 7. At about the midway point, there is a pronounced cusp in the energy. As the cusp is crossed, the magnetic moments change sharply. This suggests that the charge disproportionation drives the structural relaxation, rather than vice versa. We note that the calculated energy barrier [52] along the path is about 56 meV per vanadium, lower than the barrier calculated for small polaron hopping for Li_xFePO_3 (88-108 meV) and hematite (85-120 meV) [49, 50]. While we do not suggest that this is the actual switching path, the low barrier is consistent with the possibility of electric-field-induced polarization switching.

The stabilization of a polar phase by the combination of A-site cation layering and layered charge ordering is expected to operate in other transition metal oxide superlattices, the key ingredient being stable multiple valence states with an average valence controlled by the A cations and a mechanism for screening the electrostatic energy differences of the relevant point charge arrangements. First-principles high-throughput searches should be useful in identifying promising candidate systems for further theoretical and experimental investigation.

In summary, we predict a charge-order-driven polar phase in the 1:1 superlattice composed of perovskite oxides, $LaVO_3$ and $SrVO_3$. We find three low-energy antiferromagnetic Mott-insulating states with distinct charge ordered patterns; the SCO and CCO phases with zero out-of-plane polarization and the LCO phase with a sizable out-of-plane polarization. We find that the out-of-plane spontaneous polarization of the polar phase is comparable to that of conventional ferroelectric perovskite oxides and is much larger than in other charge-order-driven ferroelectrics. It can be understood as a transfer of electrons between V ions in the transformation between up and down polarization states. The energy difference between the normal-polarization phase and ground-state phase with zero normal polarization is small and can be controlled by (001) epitaxial strain. This suggests that the normal-polarization phase can be induced by an applied electric field and that the critical field will decrease under tensile strain. Such phases are expected also to occur in other layered superlattices with transition metal ions stable in multiple valence states.

We thank C. Dreyer, R. Engel-Herbert, V. Gopalan, D. R. Hamann, H. N. Lee, J. Liu, B. Monserrat, D. Vanderbilt, M. Ye, and Y. Zhou, for valuable discussion. First-principles calculations were performed on the Rutgers University Parallel Computer (RUPC) cluster. This work is supported by ONR N00014-11-1-0666 and ONR N00014-14-1-0613.

* Electronic address: sypark@physics.rutgers.edu

[1] D. V. Efremov, J. van den Brink, and D. I. Khomskii, Nat Mater **3**, 853 (2004).
[2] J. van den Brink and D. I. Khomskii, Journal of Physics: Condensed Matter **20**, 434217 (2008).
[3] J. Young, P. Lalkiya, and J. M. Rondinelli, J. Mater. Chem. C **4**, 4016 (2016).

[4] A. Ohtomo, D. A. Muller, J. L. Grazul, and H. Y. Hwang, Nature **419**, 378 (2002), ISSN 0028-0836.

[5] P. Zubko, S. Gariglio, M. Gabay, P. Ghosez, and J. M. Triscone, **2**, 141 (2011).

[6] H. Y. Hwang, Y. Iwasa, M. Kawasaki, B. Keimer, N. Nagaosa, and Y. Tokura, Nat Mater **11**, 103 (2012), ISSN 1476-1122.

[7] C. H. Ahn, K. M. Rabe, and J.-M. Triscone, Science **303**, 488 (2004), ISSN 0036-8075.

[8] M. Dawber, K. M. Rabe, and J. F. Scott, Rev. Mod. Phys. **77**, 1083 (2005).

[9] D. G. Schlom, L.-Q. Chen, C.-B. Eom, K. M. Rabe, S. K. Streiffer, and J.-M. Triscone, Annual Review of Materials Research **37**, 589 (2007).

[10] J. M. Rondinelli, S. J. May, and J. W. Freeland, MRS Bulletin **37**, 261 (2012).

[11] H. Chen, A. J. Millis, and C. A. Marianetti, Phys. Rev. Lett. **111**, 116403 (2013).

[12] J. Chakhalian, J. W. Freeland, A. J. Millis, C. Panagopoulos, and J. M. Rondinelli, Rev. Mod. Phys. **86**, 1189 (2014).

[13] A. L. Krick, C.-W. Lee, R. J. Sichel-Tissot, A. M. Rappe, and S. J. May, Advanced Electronic Materials **2**, 1500372 (2016).

[14] T. Birol, N. A. Benedek, and C. J. Fennie, Phys. Rev. Lett. **107**, 257602 (2011).

[15] N. A. Benedek, A. T. Mulder, and C. J. Fennie, Journal of Solid State Chemistry **195**, 11 (2012).

[16] N. C. Bristowe, J. Varignon, D. Fontaine, E. Bousquet, and P. Ghosez, Nat Commun **6**, 6677 (2015).

[17] J. Varignon, N. C. Bristowe, E. Bousquet, and P. Ghosez, Scientific Reports **5**, 15364 (2015).

[18] M. Imada, A. Fujimori, and Y. Tokura, Reviews of Modern Physics **70**, 1039 (1998).

[19] S. Ishihara, Journal of the Physical Society of Japan **79**, 011010 (2010).

[20] K. Kobayashi, S. Horiuchi, R. Kumai, F. Kagawa, Y. Murakami, and Y. Tokura, Phys. Rev. Lett. **108**, 237601 (2012).

[21] K. Yamauchi and P. Barone, Journal of Physics: Condensed Matter **26**, 103201 (2014).

[22] X. He and K.-j. Jin, Phys. Rev. B **93**, 161108 (2016).

[23] M. Alexe, M. Ziese, D. Hesse, P. Esquinazi, K. Yamauchi, T. Fukushima, S. Picozzi, and U. Gsele, Advanced Materials **21**, 4452 (2009), ISSN 1521-4095.

[24] S. Iwai, S. Tanaka, K. Fujinuma, H. Kishida, H. Okamoto, and Y. Tokura, Phys. Rev. Lett. **88**, 057402 (2002).

[25] R. Pentcheva and W. E. Pickett, Phys. Rev. Lett. **99**, 016802 (2007).

[26] M. Rey, P. Dehaudt, J. Joubert, B. Lambert-Andron, M. Cyrot, and F. Cyrot-Lackmann, Journal of Solid State Chemistry **86**, 101 (1990).

[27] P. Bordet, C. Chaillout, M. Marezio, Q. Huang, A. Santoro, S.-W. Cheong, H. Takagi, C. Oglesby, and B. Batlogg, Journal of Solid State Chemistry **106**, 253 (1993).

[28] T. Yoshida, K. Tanaka, H. Yagi, A. Ino, H. Eisaki, A. Fujimori, and Z.-X. Shen, Phys. Rev. Lett. **95**, 146404 (2005).

[29] Y. Quan, V. Pardo, and W. E. Pickett, Phys. Rev. Lett. **109**, 216401 (2012).

[30] W. E. Pickett, Y. Quan, and V. Pardo, Journal of Physics: Condensed Matter **26**, 274203 (2014).

[31] G. Kresse and J. Furthmüller, Phys. Rev. B **54**, 11169 (1996).

[32] G. Kresse and D. Joubert, Phys. Rev. B **59**, 1758 (1999).

[33] J. P. Perdew, K. Burke, and M. Ernzerhof, Phys. Rev. Lett. **77**, 3865 (1996).

[34] A. I. Liechtenstein, V. I. Anisimov, and J. Zaanen, Phys. Rev. B **52**, R5467 (1995).

[35] H. Sawada, N. Hamada, K. Terakura, and T. Asada, Phys. Rev. B **53**, 12742 (1996).

[36] Z. Fang, N. Nagaosa, and K. Terakura, Phys. Rev. B **67**, 035101 (2003).

[37] S. Biermann, A. Poteryaev, A. I. Lichtenstein, and A. Georges, Phys. Rev. Lett. **94**, 026404 (2005).

[38] M. T. Czyżyk and G. A. Sawatzky, Phys. Rev. B **49**, 14211 (1994).

[39] P. E. Blöchl, Phys. Rev. B **50**, 17953 (1994).

[40] R. D. King-Smith and D. Vanderbilt, Phys. Rev. B **47**, 1651 (1993).

[41] U. Staub, G. I. Meijer, F. Fauth, R. Allenspach, J. G. Bednorz, J. Karpinski, S. M. Kazakov, L. Paolasini, and F. d'Acapito, Phys. Rev. Lett. **88**, 126402 (2002).

[42] Y. Zhou and K. M. Rabe, Phys. Rev. B **89**, 214108 (2014).

[43] I. B. Bersuker, The Jahn-Teller Effect (Cambridge University Press, 2006), ISBN 9780521822121.

[44] J. Varignon, N. C. Bristowe, and P. Ghosez, Phys. Rev. Lett. **116**, 057602 (2016).

[45] S. Okamoto, A. J. Millis, and N. A. Spaldin, Phys. Rev. Lett. **97**, 056802 (2006).

[46] A. A. Mostofi, J. R. Yates, G. Pizzi, Y.-S. Lee, I. Souza, D. Vanderbilt, and N. Marzari, Computer Physics Communications **185**, 2309 (2014).

[47] J. Bonini and K. M. Rabe, unpublished.

[48] S. Y. Park and K. M. Rabe, unpublished.

[49] T. Maxisch, F. Zhou, and G. Ceder, Phys. Rev. B **73**, 104301 (2006).

[50] N. Adelstein, J. B. Neaton, M. Asta, and L. C. De Jonghe, Phys. Rev. B **89**, 245115 (2014).

[51] The value of U is discussed in detail in the Supplementary Material.

[52] The energy barrier is proportion to the value of U, consistent with U-dependent energy barrier in Li_xFePO_3 [49]. For U=3 eV and 5 eV, the estimated barrier is 49 and 73 meV, respectively.